Thermomechanical Properties of Nematic Liquid Crystal Elastomers

Senior Thesis by
Alice Kutsyy

In Partial Fulfillment of the Requirements for the
Degree of
Bachelor of Science in Mechanical Engineering

CALIFORNIA INSTITUTE OF TECHNOLOGY
Pasadena, California

2024

Alice Kutsyy
ORCID: 0009-0004-7970-1535

ACKNOWLEDGEMENTS

I would like to express my deepest gratitude to Professor Kaushik Bhattacharya for providing me with the opportunity to conduct this research. His guidance and support have been instrumental in the completion of this work.

I would also like to thank my graduate mentor Adeline Wihardja for her invaluable contributions to this project. I have benefited immensely from her guidance in the laboratory and her care and expertise in her mentorship.

I am grateful to the Caltech MCE division and all of the professors within it for all they have taught over the past 4 years. I have learned so much in each and every one of my classes and I am so fortunate to have had this opportunity.

I am extremely grateful for Erin Burkett at the Hixon Writing Center who offered me invaluable guidance throughout the writing process.

I could not have done this without the support of my incredible parents, Vadim and Irene Kutsyy - for hanging out with me on the phone when I was in the lab late at night, for providing me reassurance and support when I felt frustrated or stuck, and for being overall incredible parents. And of course, I am so thankful to my kitten Moca for being the cutest emotional support.

ABSTRACT

Liquid crystal elastomers (LCEs) are materials formed by cross-linking crystal mesogens into a flexible polymer network, and they display soft behavior and undergo large, reversible strains. The mesogenic order determines material properties, causing coupling between temperature, liquid crystalline order, and deformation, which leads to temperature-based actuation. LCEs have important applications in soft robotics and medical devices, so attempts have been made to theoretically model their behavior in order to develop new use cases. One such model, developed by Lee (2021), identifies regions of liquid crystal orientation and has agreed with initial experimental data (Lee et al., 2023). This thesis aims to characterize the behavior of isotropic-genesis polydomain LCEs across various temperatures, strain rates, and crosslinking densities and further test the model by comparing the experimental data against it.

Tensile tests were run across five strain rates (10^{-1}/s, 5×10^{-2}/s, 10^{-2}/s, 5×10^{-3}/s, 10^{-3}/s), three temperatures (26°C, 55°C, 90°C), and two crosslinking densities (50 mol%, 25 mol%). A custom tensile rig with a heated chamber made by Lee (2021) was modified for the purpose of this thesis to allow for digital image correlation and trials across temperatures.

These tensile tests revealed that stiffness increased with faster strain rates, and, as temperature increased, soft behavior was reduced at 55°C and vanished at above the nematic transition temperature. Additionally, residual strain decreased with increasing temperature, at ~1.5 at 26°C, ~0.75 at 55°C, and ~0.1 at 90°C. Reducing the crosslinking density more than doubled the strain at failure and drastically increased the region of soft behavior.

Experimental data across three strain rates (10^{-2}/s, 5×10^{-3}/s, 10^{-3}/s), three temperatures, and at 50 mol% crosslinking density were compared against the model developed by Lee (2021). The soft behavior of the LCE was generally well characterized by the model, however, the model deviated from experimental data above two strain, as the Neo Hookean-based model was unable to capture strain hardening. Since higher temperature trials were run to lower strains, the model was able to better capture the full behavior of the LCE at higher temperatures, even with the loss of soft behavior at 90°C. This model is therefore a useful tool for modeling LCE soft behavior across various temperatures.

TABLE OF CONTENTS

LIST OF ILLUSTRATIONS

LIST OF TABLES

Chapter 1

INTRODUCTION

Liquid crystal elastomers (LCEs) are a class of stimuli-responsive soft materials that exhibit both liquid crystalline order and rubber elasticity. Due to their unique properties, LCEs have applications in artificial muscles, soft robotics, drug delivery, stretchable membranes, and more. LCEs are a good candidate material for artificial muscles as they are able to withstand large, repeated deformation and can be actuated. Work has been done to create photo-actuated LCEs for use as artificial muscles, with the eventual goal to create neuronally-actuated LCEs (Kim et al., 2022). Soft robotics aims to incorporate soft materials into robots to mimic animal movement patterns, increase the safety of human-robot interactions, and increase the flexibility and shock absorption of the robot. The ability for LCEs to respond to various external stimuli and to dissipate energy makes soft robotics a promising application. LCEs have been used to develop an electrically-actuated inchworm-inspired crawling robot, and the high power amplification of LCEs was utilized in creating a jumping soft robot (Fernandes Minori et al., 2022; Song et al., 2022).

LCEs are formed by cross-linking crystal mesogens into the underlying polymer backbone. An early LCE synthesis method was a platinum-catalyzed hydrosilylation reaction introduced by Finkelman and Bergmann in 1997 and was later followed by polyesterification and epoxy-based synthesis reactions (Saed et al., 2016). Difficulty attaining high-purity starting materials and the reliance on random cross-linking led to poorly defined network structure and difficulties determining consistent LCE properties using early methods (Saed et al., 2016). Recent synthesis methods have produced more uniform LCE networks at larger scales, allowing the properties to be better understood and modeled (Lee et al., 2023; Saed et al., 2016).

Nematic, smectic, and cholecteric order LCEs have all been synthesized and studied; more details about each can be found in Warner and Terentjev (2003). For this thesis, I focus on the most widely studied class of LCEs: isotropic-genesis polydomain LCEs (I-PLCE). The LCEs studied are nematic, meaning they have stiff, rod-like mesogens, show long-range order, and exhibit significant deformations and shape changes due to changes in the mesogenic order. Figure 1.1a shows the difference between a polydomain and monodomain LCE. In a monodomain sample, the meso-

gens director is constant across the entire sample, while the polydomain sample has regions of mesogenic order. Both types of LCEs are thermotropic, meaning they display temperature-sensitive mesogenic orientation, leading to temperature-actuated shape changes. Figure 1.1b depicts the mesogens of a thermotropic LCE as it is heated. When heated above the nematic transition temperature T_{ni} (around 85°C), the mesogens become unordered, or isotropic. Isotropic-genesis specifies that the specimens are crosslinked in the isotropic state, and local symmetry-breaking as the samples cool below T_{ni} creates complex director patterns.

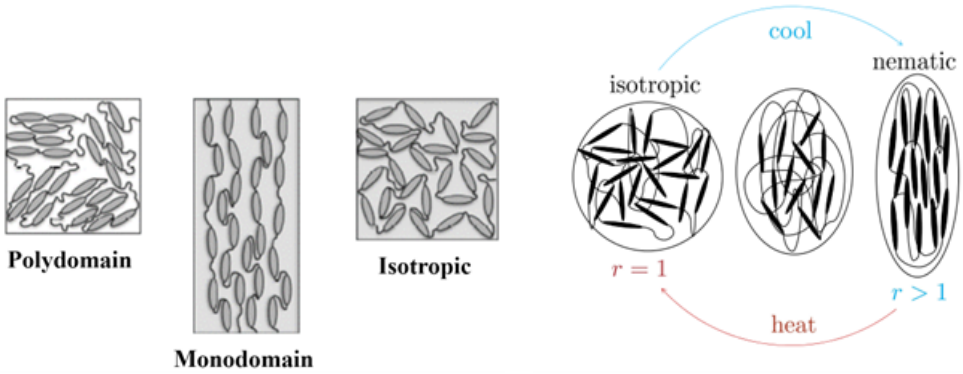

(a) (b)

Figure 1.1: Mesogen orientation across (a) different synthesis methods (modified from Saed et al. (2016)) and (b) during the nematic-to-isotropic transition with temperature (from Lee (2021)).

An important property of LCEs is soft behavior. Figure 1.2 shows a stress-strain curve for an I-PLCE below T_{ni}. The labeled plateau stress refers to the region of soft behavior, where strain increases with little added stress. When a polydomain LCE is loaded in uniaxial tension, the mesogens first reorient into the direction of stress, elongating the sample. This is known as the polydomain-to-monodomain transition and causes soft behavior (Wihardja, 2023). Once the mesogens are reoriented, the stress-strain curve slopes upward, showing the elastic response of the material as the polymer backbone stretches. Monodomain samples stretched perpendicular to the mesogen director also undergo a mesogenic reorientation where the material temporarily forms bands (known as stripe domains) to satisfy no-shear boundary conditions (Lee, 2021; Lee et al., 2023). When unloaded from high strain, the LCE returns to a residual strain (labeled in Figure 1.2) until heated above the transition temperature, at which point it reforms into its original shape and size.

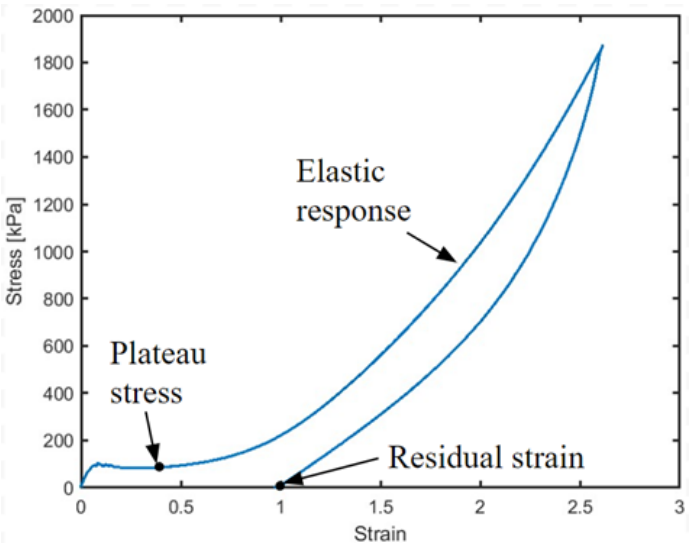

Figure 1.2: Stress-strain curve demonstrating LCE soft behavior. Plateau stress, elastic response, and residual strain are labeled.

It is important to be able to theoretically model LCE behavior in order to advance new applications. Several of these models have been developed previously. The classic model, known as the Bladon-Terentjev-Warner (BTW) model is derived from Gaussian chain modeling and shows material behavior for small and moderate stretches. However, it fails to characterize stiffer LCE behavior under significant stretch. Another model developed by DeSimone and Dolzmann captures the stripe domain formations through relaxation of the BTW model but still is unable to describe how nematic elastomers behave under high-stretch conditions. More recently, a model developed in Lee (2021) focuses on the behavior of non-ideal isotropic-genesis polydomain nematic elastomers. This model is a macroscopic, homogenized model that features internal variables concerned with the microstructures in order to capture macroscopic behavior. The agreement of this model with experimental data has been investigated in Lee et al. (2023) and the model is able to capture the behavior of these materials with only 7 input variables. However, the experiments were done at room temperature and at only one strain rate.

The necessity to test models over a variety of parameters stems from LCEs being highly tunable materials, so many different parameters will affect the material response shown in Figure 1.2 above. At low temperatures, stress will reorient the mesogens, giving rise to soft behavior and allowing large strains before failure. However, above T_{ni}, the sample becomes isotropic, lacking mesogenic order and therefore significantly changing the material response and stiffness. Beyond temper-

ature dependency, greater crosslinking density decreases soft behavior and strain at failure and increasing loading rate stiffens material response (Lee et al., 2023; Saed et al., 2016).

The objective of this thesis is therefore to characterize the behavior of I-PLCEs across different temperatures, strain rates, and crosslinking densities by performing linear tensile experiments in a heated chamber. This characterization will then be used to compare Lee's model across this wider range of parameters. I begin by characterizing the thermo-mechanical properties of isotropic-genesis polydomain LCEs at five strain rates, three temperatures, and two cross-linker densities. I then compare the material response to the model developed by Lee (2021), to see how the model's behavior varies across parameters.

Chapter 2

METHODS AND MATERIALS

2.1 Liquid Crystal Elastomer Synthesis

This thesis seeks to examine the properties of main-chain LCEs, where mesogens are incorporated directly into the polymer backbone. Mesogens, which are the basis of LC domains, consist of two or three linearly connected aromatic rings with flexible ends (Saed et al., 2016). Main-chain LCEs, as opposed to side-on LCEs, show direct coupling between the mesogenic order and the conformation of the polymer backbone (Saed et al., 2016). This direct coupling results in greater mesogen orientation, mechanical anisotropy, and strain actuation (Saed et al., 2016).

The synthesis process performed in this thesis is well documented and further detailed in both Saed et al. (2016) and Lee (2021), and a summary is provided below. Since the goal is polydomain samples, HHMP is omitted, and the samples are not UV crosslinked. The chemicals used, their purpose, formulas, and manufacturers are summarized in Table 2.1. Appendix A gives a printable sheet to document the synthesis process while in the lab.

Table 2.1: Details of synthesis chemicals.

Chemical Name	Purpose	Full Chemical Formula	Manufacturer
RM257	Di-acrylate mesogen	1,4-Bis-[4-(3-acryloyloxypropyloxy) benzoyloxy]-2-methylbenzene	Wilshire Technologies
EDDET	Di-thiol spacer	2,2'-(ethylenedioxy) diethanethiol	Sigma Aldrich
PETMP	Tetra-thiol crosslinking	Pentaerythritol tetrakis (3-mercaptopropionate)	Sigma Aldrich
DPA	Catalyst	Dipropylamine	Sigma Aldrich
Toluene	Solvent	Toluene	Sigma Aldrich

The synthesis procedure will be laid out below. First, I took two 40 mL glass vials and labeled them "Main" and "Catalyst". In "Main", I combined 2774.5 µL of

Toulene and half of the RM257 (3 g), then heated the vial on an 80°C hotplate, swirling occasionally until crystals were dissolved. I added the remaining RM257 (3 g) and placed the solution back on the hotplate until all the crystals were fully dissolved. Meanwhile, I combined 37.12 µL of DPA and 1444.5 µL of Toluene in "Catalyst". Once dissolved, I removed "Main" from the heat and added PETMP and EDDET (the amounts varied based on the desired crosslinking density). I vortex mixed "Catalyst" then added 998 µL of the catalyst solution into "Main". I vortex mixed "Main" for 20 seconds, loosened the cap, and placed the vial in a 71.1 kPa vacuum for 45 seconds. If the solution was cloudy or had suspended crystals, I placed it back on the hot plate until the crystals were fully dissolved and the solution was clear. The quantities of each chemical used for 50 mol% and 25 mol% crosslinking density samples are summarized in Table 2.2. This batch amount produced 13 samples, however, the quantities can be doubled to produce more.

Table 2.2: Chemical quantities used for synthesis at two different crosslinking densities.

Chemical	50 mol% Crosslinker	25 mol% Crosslinker
RM257	6 g	6 g
EDDET	721.3 µL	1082.0 µL
PETMP	1.083 g	0.8123 g
DPA	37.12 µL	37.12 µL
Toluene	4219.0 µL	4219.0 µL

Once made, the solution was pipetted into custom CNCed HDPE molds, depicted in Figure 2.1. The curved dogbone shapes used in the molds were adapted from ASTM D914 and ISO 37 standards. The dogbone was scaled down to 2 mm deep and 5 mm wide at the narrowest section to fit the available testing rig. The dogbone shape was also curved to ensure the highest stress concentration was in the central region (the region captured by image analysis), as well as to prevent snagging and breaking at the corners when demolding.

Figure 2.1: HDPE curved dogbone molds used for LCE synthesis.

The molds were then left at room temperature in a fume hood for 12 hours, then moved into a vacuum oven under a 71.1 kPa vacuum at 80°C. After 24 hours, I released the vacuum and turned the oven off. The samples were allowed to cool slowly within the chamber for 3 hours, followed by 30 minutes of cooling at room temperature before I removed them from the molds. I then briefly placed the samples on a hot plate until they turned clear and shrank back to their original size to remove any deformation caused by demolding.

Finally, I taped down both ends of the sample, which I then spray painted, first with a base layer of white before speckling with black to allow for digital image correlation. I used flat spray paint to reduce glare and was careful to choose a paint that could withstand 90°C testing, as melting would both cause issues with image correlation and present a health hazard.

Initial test results were used to modify the synthesis process to increase consistency. Figure 2.2 shows tension tests to failure (defined as sample fracture) at room temperature with a strain rate of 10^{-2}/s for all batches made with a crosslinking density of 50 mol%. The first three batches made displayed a much softer response and are inconsistent. To address this, I began measuring PETMP by weight rather than volume in a micropipette, as PETMP is very viscous and the micropipette only moved approximately 75% of the desired volume. The next 5 batches were much more consistent. All results presented later are from these weighed batches.

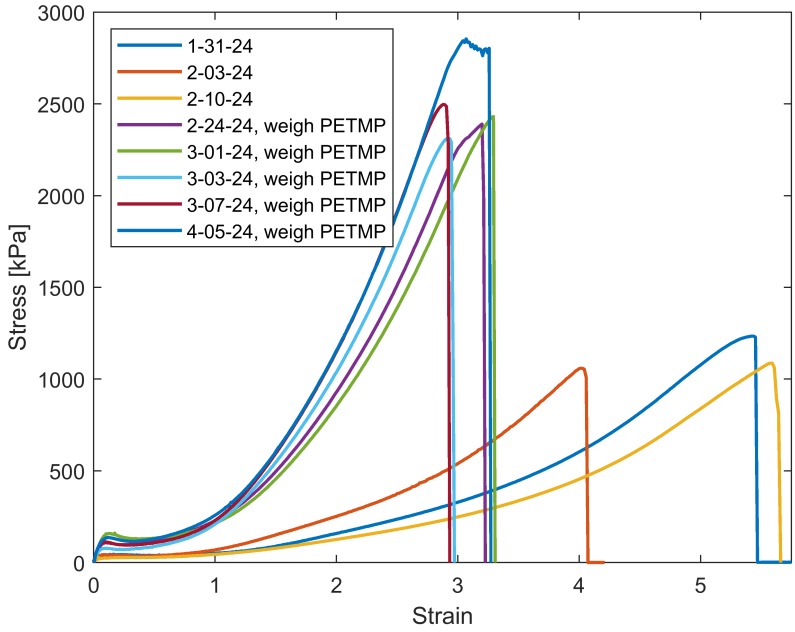

Figure 2.2: Tension test to failure across all 50 mol% crosslinking density batches. Initial batches showed inconsistent behavior, leading to changes in the synthesis method.

Additional tests were performed on one batch to verify the effects of spray paint and time on the samples, shown in Figure 2.3 below. The tension tests were performed to failure at room temperature with a strain rate of 10^{-2}/s across a single batch with 50 mol% crosslinking density. Here, T represents the time the samples were demolded, and we can see that as more time elapsed, the samples became stiffer. Thus, all tests were run between 2 and 14 hours after demolding to decrease this time-dependent change in properties. Additionally, we can see that the lack of spray paint made the sample less stiff (although there was significant slip present, as indicated by the flat region just before failure). The variation between sprayed and unsprayed was larger than the variation between multiple identical samples (depicted in blue); therefore, spray paint was applied to all tested samples, regardless of whether or not image analysis was being utilized, in order to increase consistency.

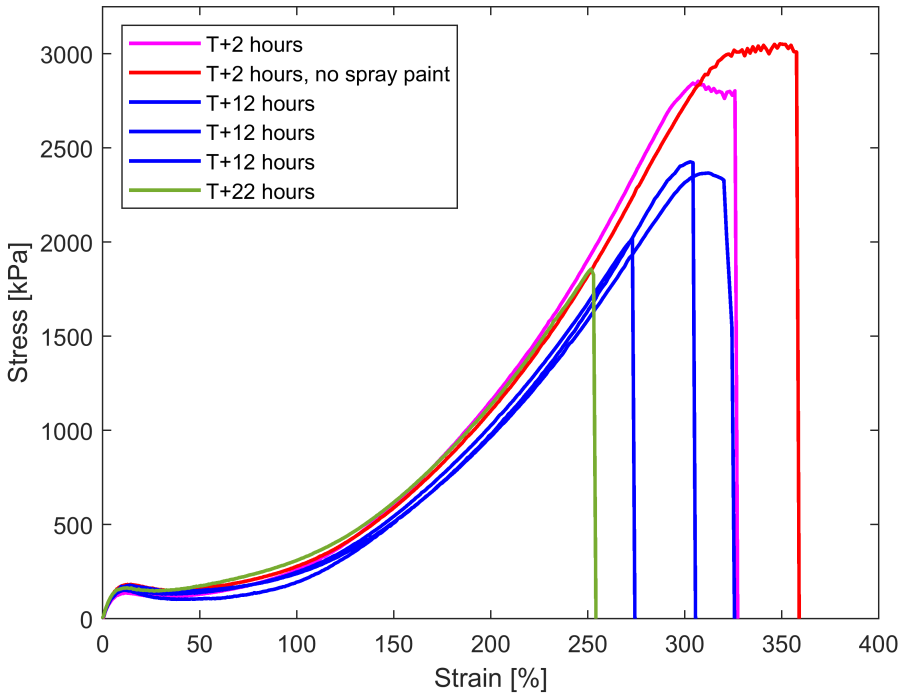

Figure 2.3: Effect of time and spray paint on LCE behavior. Due to noticeable changes in material behavior, all subsequent trials run were with spray painted and 2-14 hours after demolding to increase consistency.

2.2 Tensile Test Rig Design

Tensile tests are performed at various strain rates, temperatures, and crosslinking densities to probe the behavior of isotropic-polydomain LCEs (I-PLCEs). I used a custom-made rig modified from Lee (2021), shown in Figures 2.4 and 2.5 below. The system is made up of the following subsystems: chamber assembly (chamber with windows, stationary bottom clamp, and moving pullrod with clamp), heating (heaters, RTD sensors, and temperature controller), extension (linear stage, linear stage controller, and suspension assembly), load (load cell and external power supply), optics (lighting and camera), and data acquisition (computer and DAQ). The original make and model of each component are detailed in Lee (2021), and all modifications I made are explained and detailed below.

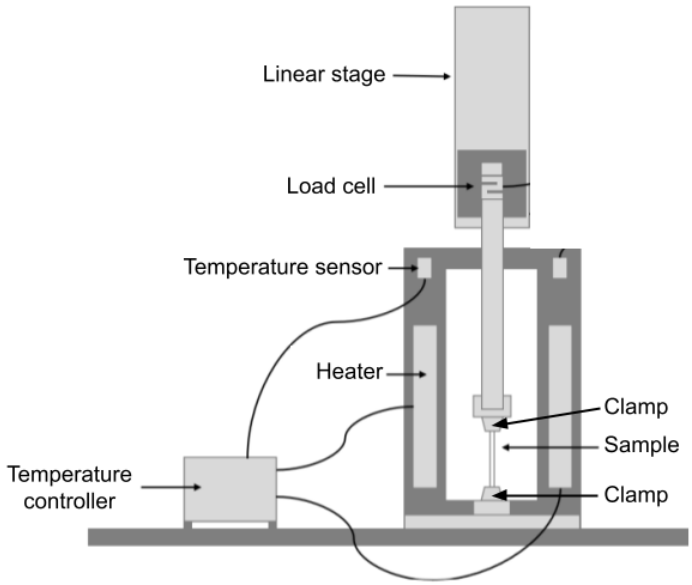

Figure 2.4: Schematic of experimental setup.

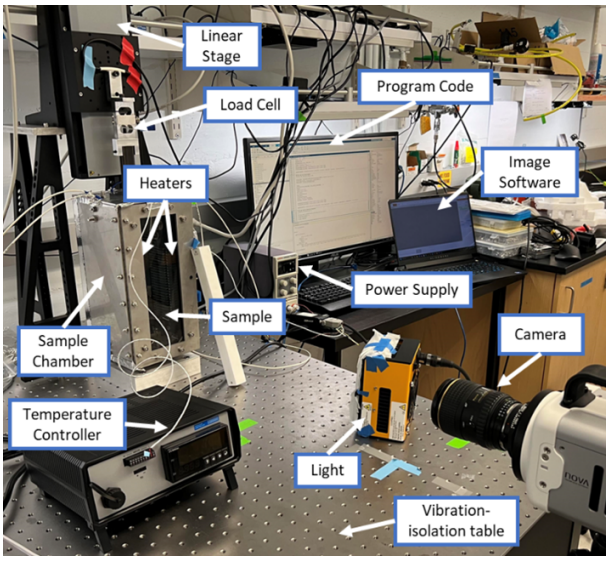

(a)

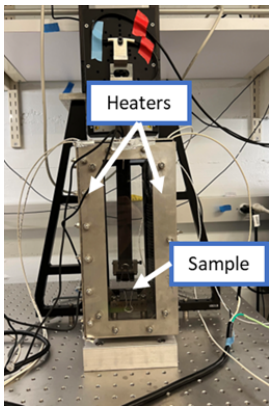

(b)

Figure 2.5: Pictures of the experimental setup, showing (a) the general setup and (b) the heated chamber, modified from Lee (2021). The light, temperature controller, and camera were added to perform DIC analysis and for greater temperature stability.

The original tests run on this rig did not include image analysis. To perform digital image correlation (DIC), the samples were speckled, and a continuous light source and NOVA-S128M camera (used in conjunction with the Photron FASTCAM Viewer software) were added. This camera was chosen as it had high resolution (1024 by 1024 pixels), was able to record at 2 or 5 frames per second, did not have

automatic image smoothing features, and was already available to the lab. However, the camera was only able to record 5437 frames at a time, limiting the slowest test to a strain rate of 10^{-3}/s. Image correlation was done in the VIC-2D software. DIC analysis gave larger strain values than the values read from the linear controller through MatLab (example difference shown in Figure 2.6a below). This is because the DIC analysis captures only the central region of the sample, chosen to minimize edge effects and slip. The curved dogbone molds shown in Figure 2.1 are thinner in the center and therefore deform more in the region of interest. The DIC analysis also allowed for visualization of how the strain concentration on the sample evolved over time, depicted with the gauge section demarcated in Figure 2.6b. DIC analysis was not used on 25 mol% trials at room temperature, as large strains caused poor image correlation.

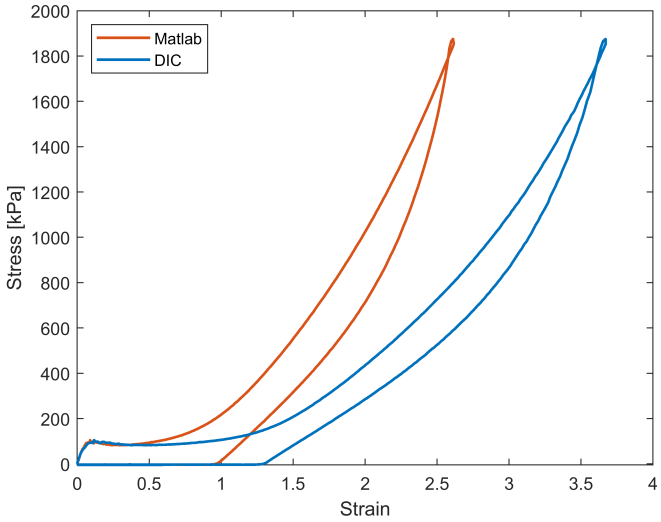

(a)

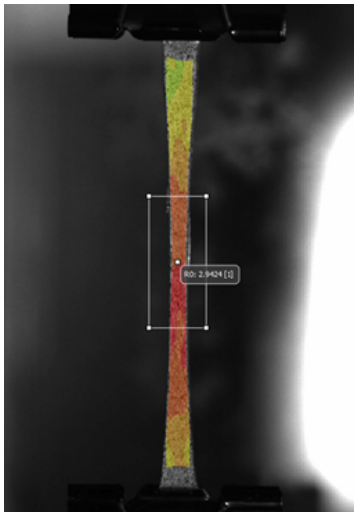

(b)

Figure 2.6: DIC analysis yielded larger strain values than Matlab recorded data, as seen in (a) DIC vs Matlab sample plot, due to a higher strain concentration in (b) the demarcated region of interest.

The original Omega CSI32RTD-C24 temperature controller used in Lee (2021) was broken and had been discontinued, so it was initially replaced by two Inkbird ITC-308 controllers (one per heater). However, these controllers led to large temperature fluctuations and were replaced with the more stable, though more expensive, Omega CS8DPT Benchtop controller. The temperature over time for both controllers is shown in Figure 2.7 below. Additionally, the thermal chamber was insulated with 3M High-Temperature Flue Tape to seal large gaps and help maintain the temperature. Heated tests were run at both 55°C and 90°C. The largest recorded temperature

fluctuation was 8°C during the slowest strain rate trial (10^{-3}/s) at 90°C, which was sufficient as the sample remained above T_{ni} throughout the test.

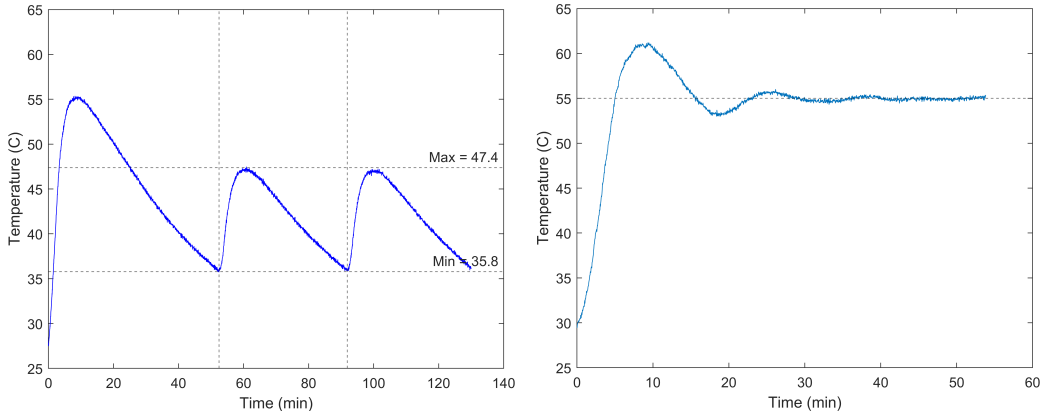

(a) (b)

Figure 2.7: Temperature fluctuation over time using an (a) two Inkbird temperature controllers and (b) an Omega temperature controller.

To perform the tensile tests, the main code found in Appendix B was run, following the embedded prompts. Each test began by measuring the sample properties and inputting the desired maximum engineering strain. I then clipped the sample into the chamber at room temperature and set the temperature controller to the desired temperature. Once heated, I set the camera to record and ran the move routine. After the test, I opened the chamber and allowed it to cool to room temperature before the next trial. The MatLab program outputs a stress-strain plot with engineering strain, so post-processing was done to convert to Lagrangian strain, and the DIC data was processed in VIC-2D and plotted against stress.

Two areas should be improved for future tests. First, the back panel should be removed and replaced with a solid, hinged panel, similar to the front panel. The back glass caused reflections, which in turn led to issues with image correlation. The hinges would help cool the chamber; after a 90°C run, the chamber took 22 minutes to return to room temperature. Opening the back panel would allow air to flow through the chamber, therefore drastically decreasing cooling time.

Second, and more importantly, the clamps need to be replaced. For this thesis, the LCE samples were clamped between binder clips, which led to slip issues at room temperature. Additionally, this caused a stress concentration at the top and bottom of the sample (see Figure 3.5), and many samples (particularly those at high temperatures) broke at either edge, rather than in the center. Looking at trials to

failure, 71% of trials failed at the edge (58% at room temperature, 67% at 55°C, and 100% at 90°C). When heated above T_{ni}, multiple samples tore without any applied load, as the binder clamp cut through the softened material during preheating. One solution would be to clamp the ends of the LCE between flat plates, spreading the stress across a larger area. A CAD model of flat, textured clamps is shown in Figure 2.8, taken from a different rig within the lab and easily modifiable for this setup.

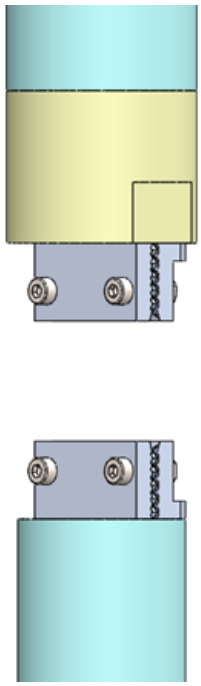

Figure 2.8: Model replacement clamps to reduce stress concentrations along the sample edges.

Chapter 3

RESULTS

LCE tensile tests were run at five strain rates (10^{-1}/s, 5×10^{-2}/s, 10^{-2}/s, 5×10^{-3}/s, 10^{-3}/s), three temperatures (room temperature (RT) at 26°C, 55°C, 90°C), and two crosslinking densities (50 mol%, 25 mol%). Unless otherwise noted, all trials in a graph are from the same synthesis batch, and all strains are Lagrangian strains.

3.1 Crosslinking Density 50 mol%

Tensile Tests to Failure

Tensile tests were first conducted to failure to examine general trends across parameters and to determine the maximum strain for load-unload trials. DIC was not performed on failure trials, therefore, Figure 3.1 below shows only the MatLab collected Lagrangian strain data across all three temperatures at 50 mol% crosslinking density.

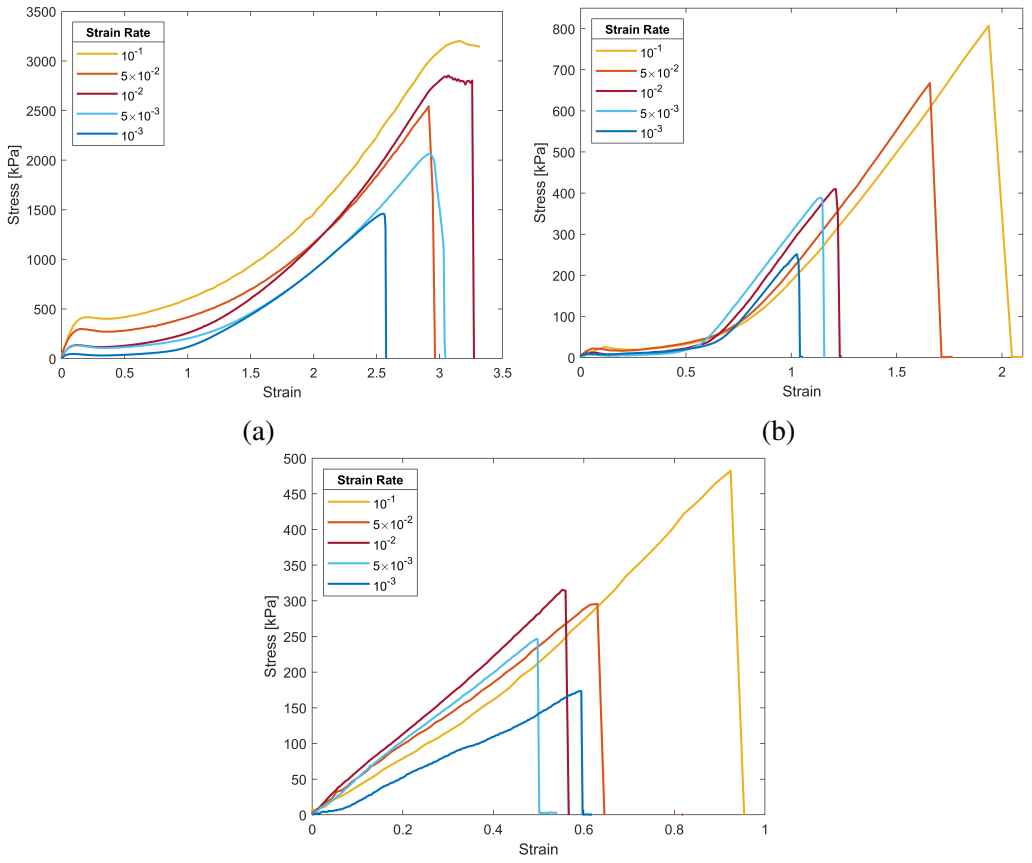

Figure 3.1: Tensile tests to failure at (a) room temperature, (b) 55°C, and (c) 90°C for samples with 50 mol% crosslinking density.

The effect of temperature on soft behavior is visible when comparing across plots in Figure 3.1. At room temperature, soft behavior is visible until ~1 strain, whereas at 55°C soft behavior is present until ~0.6 strain, and soft behavior is not seen at 90°C. The strain at failure decreases with strain rate within each temperature, except for 10^{-3}/s at 90°C, which failed at an unexpectedly high strain. It is important to note that I terminated the 10^{-1}/s trial at room temperature before failure to avoid potential damage to the rig, as the linear stage began ringing from the high stress and loading rate. Similarly, the 10^{-2}/s trial at room temperature began slipping out of the clips, causing both the plateau before failure seen in Figure 3.1a (red curve) and for the program to record an artificially large strain at failure. The expected trend is decreasing stiffness with slower strain rates, which is seen at room temperature. However, the 10^{-1}/s, 5×10^{-2}/s, and 10^{-2}/s trials at 55°C and the 10^{-1}/s and 5×10^{-2}/s trials at 90°C show a reversed trend, where stiffness increases with decreasing strain rate.

The failure tests were run to determine the maximum strain for subsequent load-unload curves. The goal was to choose a maximum strain that captures the general behavior without risking failure. Therefore, the maximum strain value was chosen in the elastic response region (defined in Figure 1.2). The maximum strain values are listed in Table 3.1 below and depict the same general trends as discussed above.

Table 3.1: Maximum Lagrangian strains for load-unload curves, determined by examining trials to failure.

	10^{-1}/s	5×10^{-2}/s	10^{-2}/s	5×10^{-3}/s	10^{-3}/s
Room Temperature	2.031	2.625	2.625	2.625	2.031
55°C	1.305	0.861	0.861	0.625	0.625
90°C	0.625	0.48	0.345	0.345	0.345

Tensile Tests at Room Temperature

Two batches of room temperature load-unload trials were run and the data is displayed in Figure 3.2 below. It is important to note that the endpoints in the first batch exceed those in Table 3.1, but directly comparing both batches in Figure 3.2c shows the shape of the curves is unaffected by the endpoints.

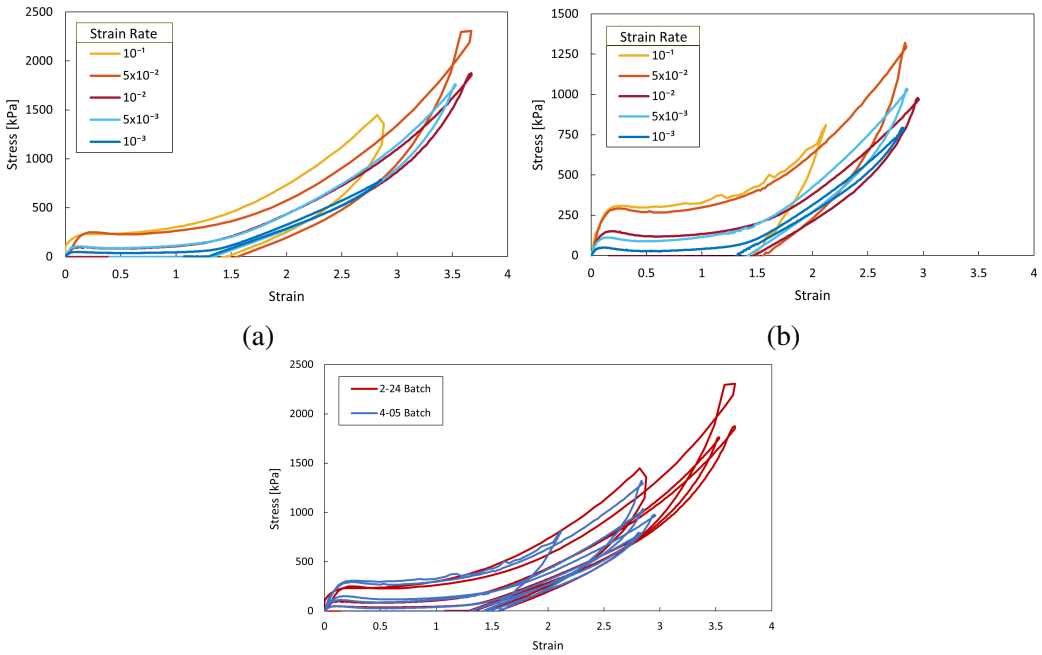

Figure 3.2: Room temperature load-unload trials across strain rates for 50 mol% crosslinking density, showing the (a) 2-24-24 batch, (b) 4-05-24 batch, and (c) comparison across batches.

Similar to the room temperature failure trial in Figure 3.1a, both batches show decreasing stiffness with slower strain rates. Additionally, the residual strain was consistently ~1.5, regardless of strain rate or batch. Looking closely at the peak of each curve, many of the higher strain rate trials show a loop at the top, most clearly seen in the 5×10^{-2}/s trial in Figure 3.2a. This indicates that buckling occurs before shrinkage, i.e. the speed of LCE shrinkage is slower than the unloading strain rate and therefore the material first buckles before shrinking. This also explains why this is not seen in any of the 10^{-3}/s trials.

Looking at the combined trials in Figure 3.2c, we observe little difference in the magnitude or shape of the stress-strain curves across batches, aside from the maximum strains the trials were run to. The variability between the batches is similar to the variability seen in Figure 2.2 and does not seem to increase or decrease with strain rate.

Tensile Tests at 55°C

One batch was run at 55°C to characterize behavior at an intermediate temperature below T_{ni}, and the results are shown in Figure 3.3 below. More significant buckling is seen across all trials, and the residual strain is ~0.7 strain. The maximum stresses reached at 55°C are roughly ten times less than at room temperature, indicating that the heated samples can withstand much less applied force. The plateau stress is nearly identical between the 10^{-1}/s and 5×10^{-2}/s trials, as well as between the 10^{-2}/s and 5×10^{-3}/s trials, although soft behavior truncates sooner at lower strain rates.

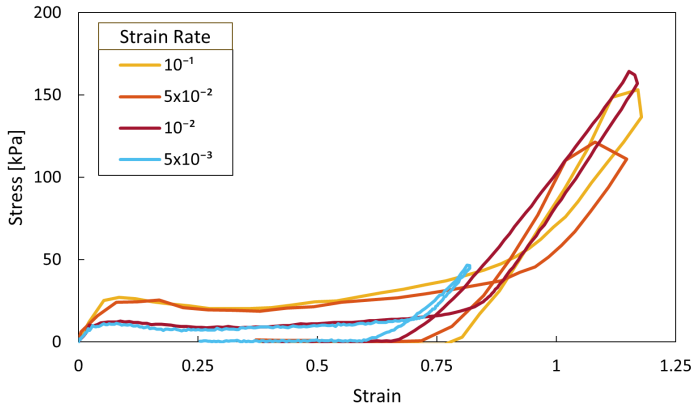

Figure 3.3: 55°C load-unload trials across strain rates for 50 mol% crosslinking density, showing the 3-01-24 batch.

Tensile Tests at 90°C

When heated to 90°C, the samples are above the nematic transition temperature and the mesogens are fully isotropic. This leads to the absence of soft behavior, as seen in both batches in Figure 3.4 below.

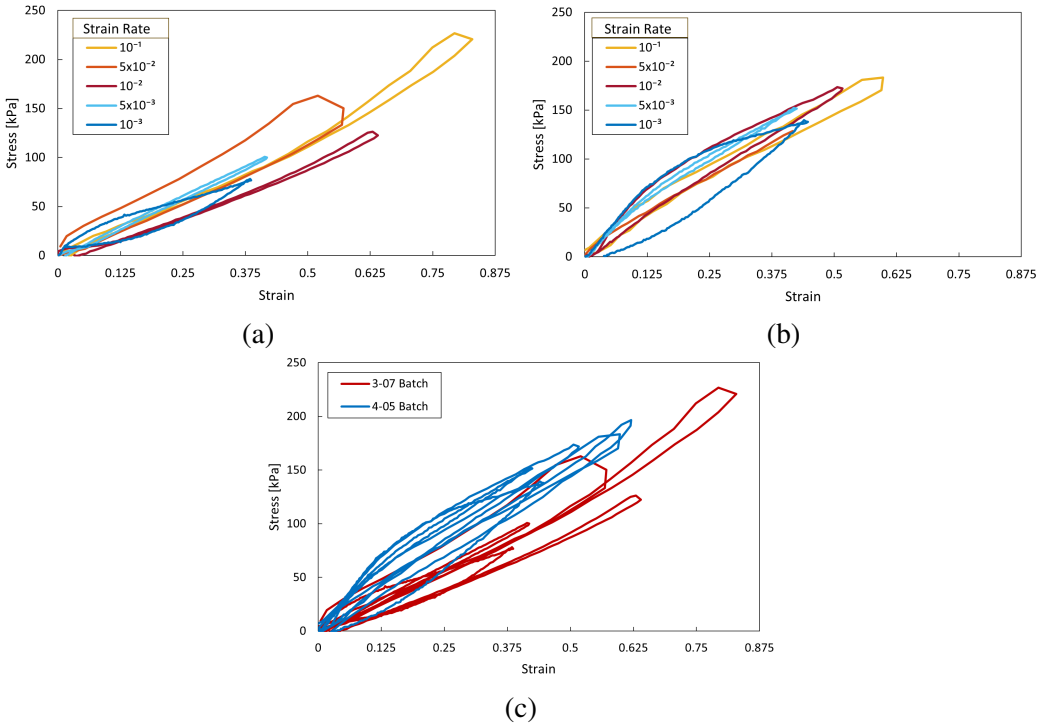

Figure 3.4: 90°C load-unload trials across strain rates for 50 mol% crosslinking density, showing the (a) 3-07-24 batch, (b) 4-05-24 batch, and (c) comparison across batches.

Above the nematic transition temperature, no soft behavior is displayed – instead, the stress-strain curve is generally linear, similar to the elastic region of typical stress-strain curves. The samples return to nearly zero strain, consistent with the typical shrinking behavior above T_{ni} that the LCE exhibits. While there is a clear distinction between the two batches in Figure 3.4c, the difference is similar to the differences seen between batches in Figure 2.2.

There is no clear trend between strain rate and stiffness, likely overshadowed by secondary effects like concentration gradients due to the clamps and slight temperature fluctuations, particularly in slower strain rate trials. Indeed, many of the samples to failure broke at the bottom, rather than in the center, and DIC imaging shows an uneven stress gradient in the samples (example trial at 10^{-2}/s shown in Figure 3.5 below).

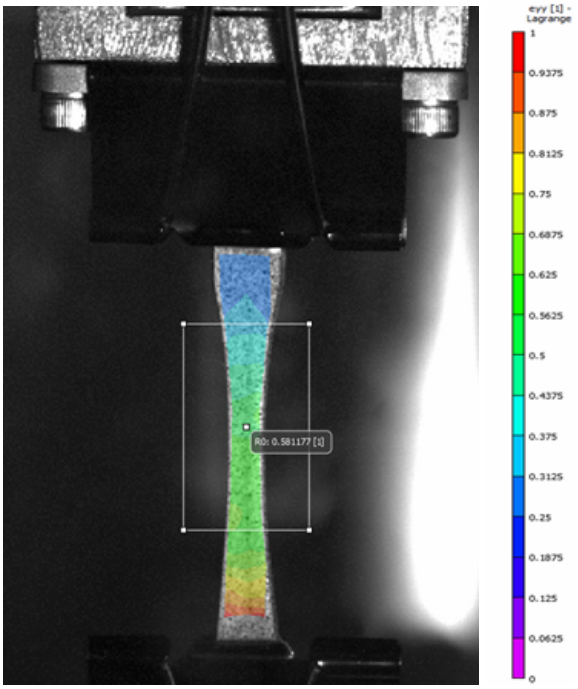

Figure 3.5: Example strain concentration gradient in a 90°C trial. The region of interest analyzed is depicted in white, and this image corresponds to a 10^{-2}/s strain rate trial on 3-07-24. Strain is greatest at the bottom, not the center as expected for uniaxial tension.

Comparison Across Temperatures

The same data can be grouped by strain rate, illustrating the effect of temperature on LCE behavior (Figure 3.6). Figure 3.6 combines data across batches, however, the difference in behavior at various temperatures are far greater than differences from batch variation.

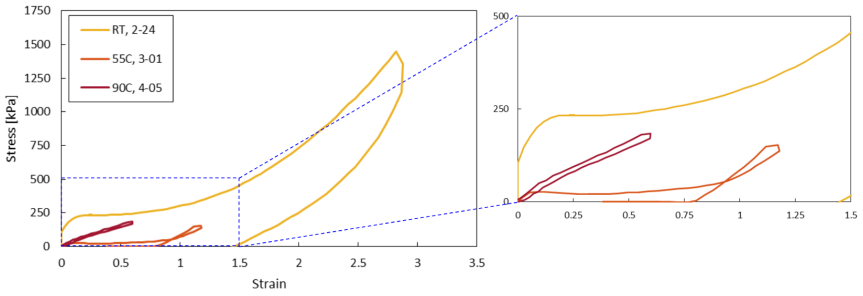

(a)

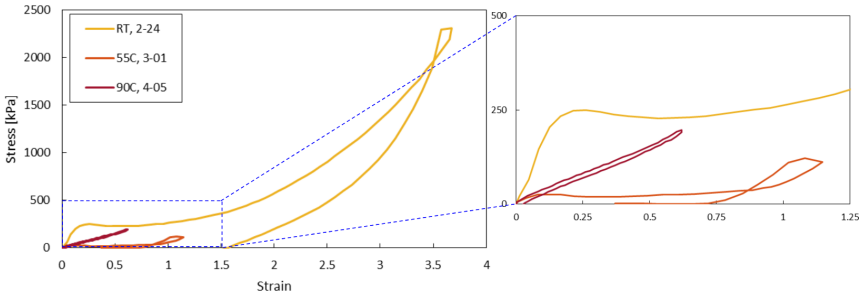

(b)

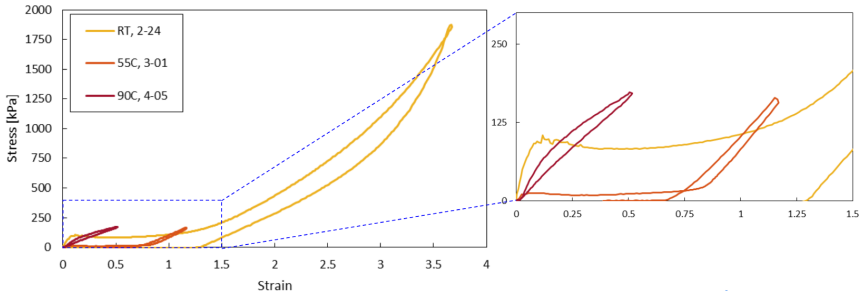

(c)

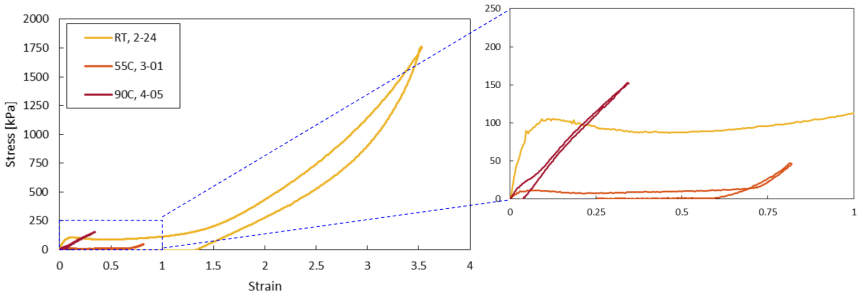

(d)

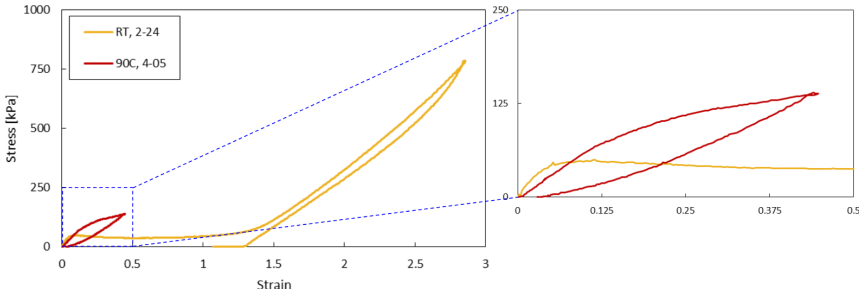

(e)

Figure 3.6: Comparison across temperatures for trials with a strain rate of (a) 10^{-1}/s, (b) 5×10^{-2}/s, (c) 10^{-2}/s, (d) 5×10^{-3}/s, (e) 10^{-3}/s.

Directly comparing the data across temperatures highlights the drastic difference in maximum stresses and strains between the room temperature and heated trials. For example, in Figure 3.6b, the 5×10^{-2} strain rate trial showed a maximum stress and strain of 2250 kPa and 3.5 at room temperature, 125 kPa and 1.125 at 55°C, and 200 kPa and 0.6 at 90°C. Interestingly, while trials run at 90°C reached lower strains than at 55°C, they withstood similar or larger stresses. Enlarging the regions of soft behavior in Figure 3.6 highlights the low plateau stress for 55°C trials, in the range of 10-50 kPa. The added heat therefore causes the polydomain-to-monodomain transition to occur at lower stresses. There is also a clear reduction in residual strain across temperatures; the residual strain decreases from ~1.5 at room temperature to ~0.75 at 55°C and ~0.02 at 90°C.

3.2 Crosslinking Density 25 mol%

The results of one batch of 25 mol% crosslinking density samples show significantly increased soft behavior (Figure 3.7).

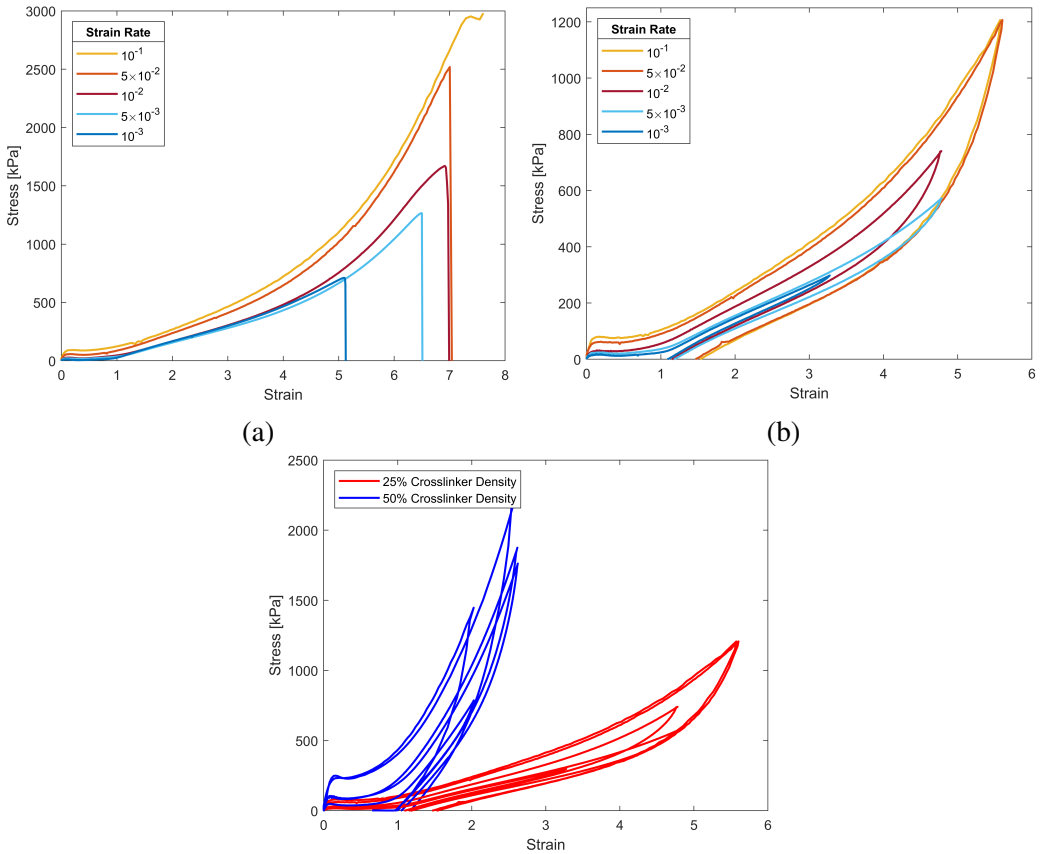

Figure 3.7: Room temperature trials for 25 mol% crosslinking density (a) to failure, (b) load-unload curves, and (c) compared to 50 mol% crosslinking.

Before analyzing, it is important to note that no DIC analysis was performed at 25 mol%, and Figure 3.7 shows the MatLab recorded data. The high strains caused large distortion of the speckles, leading to low correlation between images. Therefore, the strain values are slightly smaller than from DIC, however general trends can still be compared. Additionally, I again truncated the 10^{-1}/s trial to failure early due to ringing in the rig.

We see that these trials show decreasing stiffness with slower strain rate (Figure 3.7(a–b)), matching the trend at room temperature for 50 mol% crosslinking density. Additionally, the sample unloaded to ~1.25-1.5, which is consistent with the 50 mol% trials at room temperature (although this may be slightly lower than what would have been seen with DIC). Comparing the 25 mol% and 50 mol% crosslinking density trials directly in Figure 3.7c, we immediately see that the 25 mol% crosslinking density trials are much softer and elongate to much greater strains (5.5 vs 2). Additionally, the truncation of the soft behavior is less obvious at lower crosslinking density, as the curve gradually curves rather than having a defined transition region.

3.3 Model Comparison

One DIC stress-strain curve from each temperature and strain rate pair was taken and compared to the model. Model comparison was performed only for trials at strain rates of 10^{-2}/s, 5×10^{-3}/s, and 10^{-3}/s in order to satisfy the quasi-static approximation. The model comparison below focuses on trials at 50 mol% crosslinking density, however, the model can be modified to fit 25 mol% crosslinking trials by varying the anisotropy parameter r.

The input parameters of each model curve are found in Table 3.2, and the model is compared to the experimental data at each parameter pair in Figure 3.8.

Table 3.2: Input parameters for each model curve shown in Figure 3.8.

	Room Temperature			55°C		90°C		
	10^{-2}/s	5×10^{-3}/s	10^{-3}/s	10^{-2}/s	5×10^{-3}/s	10^{-2}/s	5×10^{-3}/s	10^{-3}/s
r	10	10	10	6	5	2.5	2	2
μ_1 (kPa)	1900	2200	2100	1600	1900	250	225	175
μ_2 (kPa)	0	0	0	0	0	0	0	0
k	2	2	2	2	2	2	2	2
α_δ (Pa)	5×10^4	9×10^4	2×10^5	4×10^3	8×10^3	10^3	10^2	2×10^5
α_λ (Pa)	$\alpha_\delta/100$	$\alpha_\delta/100$	$\alpha_\delta/100$	$\alpha_\delta/100$	$\alpha_\delta/100$	$\alpha_\delta/100$	$\alpha_\delta/100$	$\alpha_\delta/100$
c (Pa)	0.9	0.65	0.3	0.04	0.012	0.3	0.3	0.3

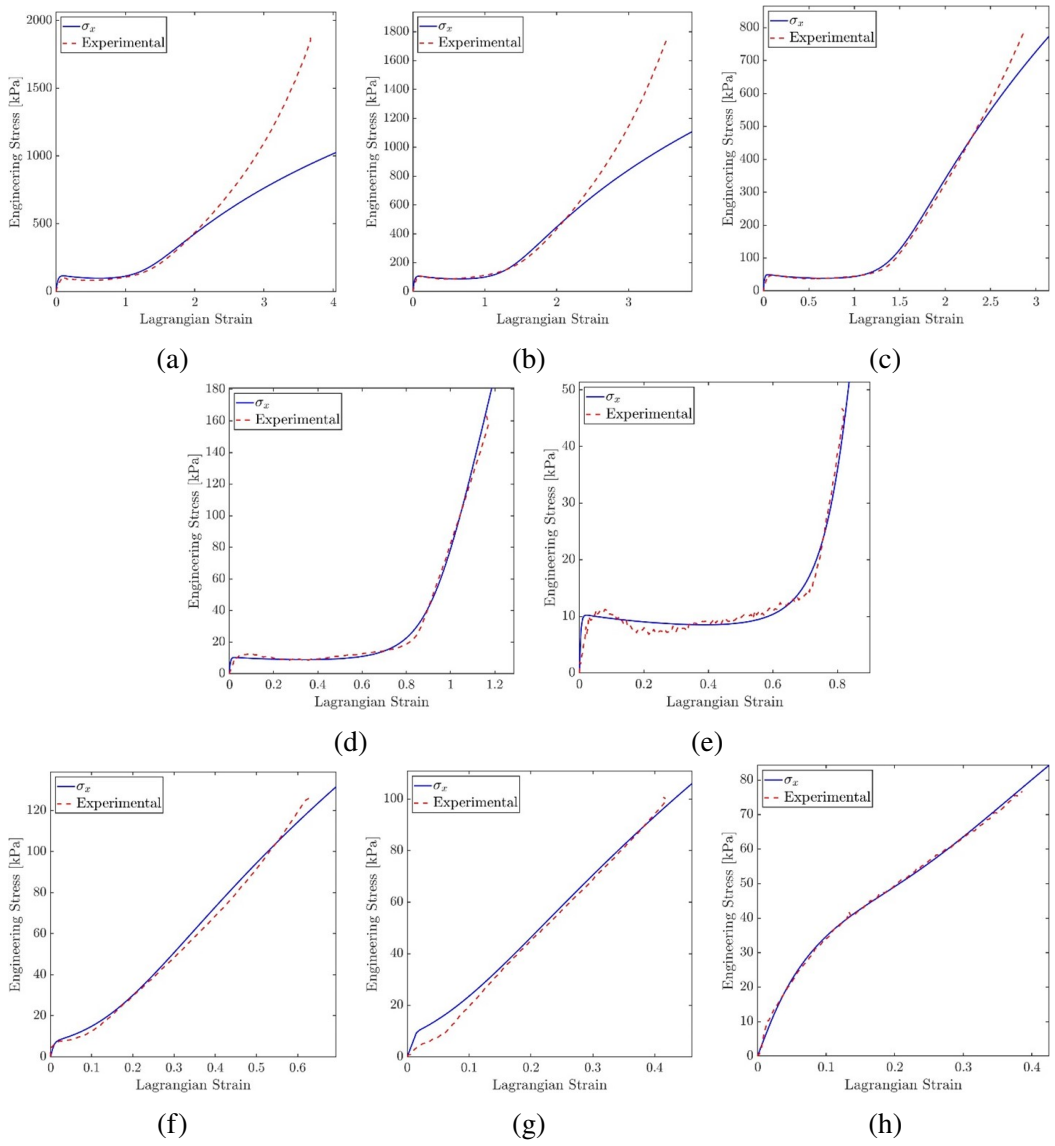

Figure 3.8: Experimental data compared to the model, for each parameter set, listed as temperature, strain rate: (a) RT, 10^{-2}/s, (b) RT, 5×10^{-3}, (c) RT, 10^{-3}/s, (d) 55°C, 10^{-2}/s, (e) 55°C, 5×10^{-3}, (f) 90°C, 10^{-2}/s, (g) 90°C, 5×10^{-3}, and (h) 90°C, 10^{-3}/s.

While generally a good fit, the model struggles to capture the behavior at high strains (>2), as seen by the room temperature trials in Figure 3.8(a–c). This issue did not affect the higher temperature trials, as the strains were kept much lower. Additionally, the model struggled to match very low strain values, with the model curve increasing rapidly at low strain and then plateauing, while the experimental curve is smoother. These trends can be seen more clearly by viewing the percent error versus strain across all parameters in Figure 3.9 below.

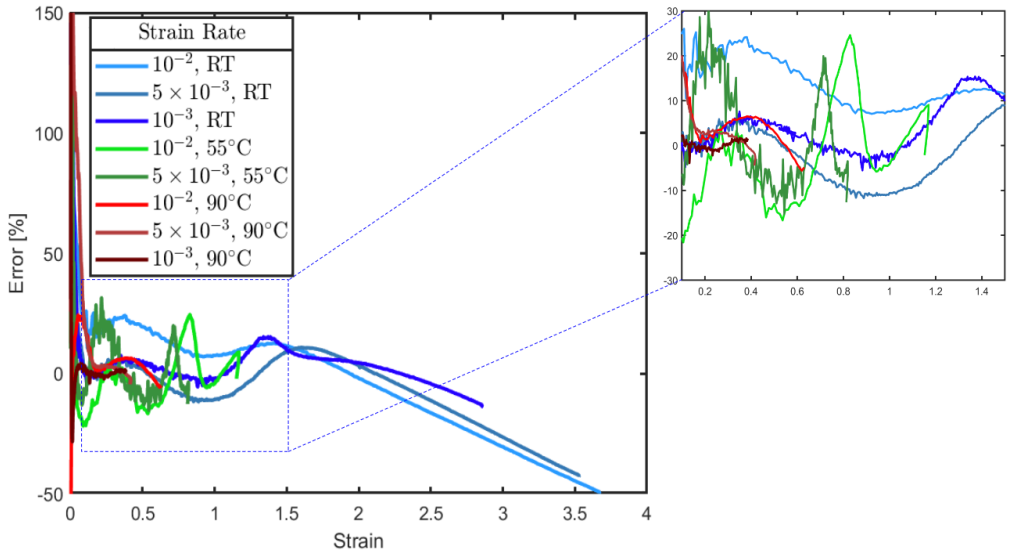

Figure 3.9: Model percent error across all parameters, where percent error is defined as (model-experimental)/experimental.

Figure 3.9 confirms the drastic overshoot at infinitesimally small strains, as well as the deviation from experimental data at strains greater than 2. The region from 0.1-1.5 strain shows more variation in the error. The error is lower for slow (10^{-3}/s) trials, as well as for 90°C trials. However, the error oscillates, generally increasing and then decreasing below zero. Looking at Figure 3.8(a–e), we can see that the model generates a flat region of plateau stress, while the experimental data has a mild curve to it and has a minimum roughly halfway through the plateau region. This difference generates the oscillation in the error plot.

Chapter 4

CONCLUSION

In this thesis, I begin by characterizing isotropic-genesis polydomain LCE behavior over various strain rates, temperatures, and crosslinking densities. At room temperature, strain hardening is visible, as stiffness increases with higher strain rates. At an intermediate temperature (between room temperature and T_{ni}), the samples fail at drastically lower strains and stresses, suggesting sub-T_{ni} temperatures still affect the mesogenic order. Above T_{ni}, the LCE is isotropic at rest and does not display soft behavior in tension, indicating that the added stress does not cause a transition to a monodomain, unlike at room temperature. Decreasing the mol% crosslinking density leads to failure at much higher strains and increased soft behavior.

Comparing the experimental data to the model from Lee (2021) illustrates how temperature and strain rate affect the model's fit. The model failed to capture high-strain behavior at room temperature, as the model's Neo Hookean basis does not account for strain hardening. At greater temperatures, the LCEs fail before this becomes an issue. The error between the model and the data is very high near zero, however, this occurs only in the first 0.1 strain and therefore does not have a significant effect on the general LCE behavior. The model is able to capture plateau stress and soft behavior well at both room temperature and an intermediate temperature, as well as non-soft behavior above T_{ni}. Overall, the model is very good at predicting the soft behavior of LCE across different temperatures and therefore is useful when looking at applications that involve soft behavior and temperature variation.

While this thesis was able to explore the model error over strain rate and temperature, DIC analysis was unable to correlate across images at low crosslinking density, so the model was not tested across different densities. Future work could repeat these trials with a greater crosslinking density to mitigate imaging issues. Additionally, an intermediate temperature between room temperature and 55°C should be tested, as the behavior at 55°C is already drastically different than at room temperature.

BIBLIOGRAPHY

Fernandes Minori, A., Jadhav, S., Chen, H., Fong, S., & Tolley, M. T. (2022). Power amplification for jumping soft robots actuated by artificial muscles. *Frontiers in Robotics and AI*, *9*. https://doi.org/10.3389/frobt.2022.844282

Kim, I. H., Choi, S., Lee, J., Jung, J., Yeo, J., Kim, J. T., Ryu, S., Ahn, S.-K., Kang, J., Poulin, P., & Kim, S. O. (2022). Human-muscle-inspired single fibre actuator with reversible percolation. *Nature nanotechnology*, *17*(11), 1198–1205. https://doi.org/10.1038/s41565-022-01220-2

Lee, V. (2021). *Theoretical, computational, and experimental characterization of nematic elastomers* [Doctoral dissertation, California Institute of Technology].

Lee, V., Wihardja, A., & Bhattacharya, K. (2023). A macroscopic constitutive relation for isotropic-genesis, polydomain liquid crystal elastomers. *Journal of the Mechanics and Physics of Solids*, *179*, 105369. https://doi.org/10.1016/j.jmps.2023.105369

Saed, M. O., Torbati, A. H., Nair, D. P., & Yakacki, C. M. (2016). Synthesis of programmable main-chain liquid-crystalline elastomers using a two-stage thiol-acrylate reaction. *Journal of visualized experiments: JoVE*, (107), e53546. https://doi.org/10.3791/53546

Song, X., Zhang, W., Liu, H., Zhao, L., Chen, Q., & Tian, H. (2022). 3d printing of liquid crystal elastomers-based actuator for an inchworm-inspired crawling soft robot. *Frontiers in Robotics and AI*, *9*. https://doi.org/10.3389/frobt.2022.889848

Warner, M., & Terentjev, E. M. (2003). *Liquid crystal elastomers*. Oxford Science Publications.

Wihardja, A. (2023). *Liquid crystal elastomers under dynamic loads* [Candidacy report, California Institute of Technology].

Appendix A

SYNTHESIS FOR 50 MOL% PETMP

Basic Information:

Name: _____

Date: _____

Molds used: _____

Mol% PETMP: _____ - IF NOT 50, MODIFY TEMPLATE

PART 1: Making and molding the samples Checklist:

- ☐ Wear PPE
  - ☐ Safety glasses
  - ☐ Gloves
  - ☐ N-95
  - ☐ Closed-toe shoes
- ☐ Clean mold with IPA, DI water, Kim wipe
- ☐ Label 2 vials: M (main), Cat (catalyst)

Hot plate dial level: _____

Time synthesis started: _____

Item	Expected weight (g)	Micropipette volume (µL)	Actual weight, subtotal (g)	Leftover on weigh boat or paper (g)	Actual weight, final (g)	% error
RM257	6 g					
Toluene	(2.4 g)	2774.5 µL				
Time on hot plate:						
Make catalyst solution in separate vial:						
DPA	(0.0275 g)	37.12 µL				
Toluene	(1.25 g)	1444.5 µL				
Total catalyst solution		988.4 µL				
Mix catalyst solution on vortex mixer						
PETMP (50 mol%)	1.083 g	(845.5 µL)				
EDDET	(0.808 g)	721.3 µL				
Vortex mixer for 20 seconds						
Vacuum oven at 20in Hg at room temperature for 45 seconds						

Did the sample recrystallize and need a 2nd time on the hot plate? _____

Solution appearance (cloudy, clear, undissolved solids?): _____

Photo of solution in vial and in molds? _____

Time, after poured into molds and placed in fume hood: _____

Number of samples made: _____

Clean-up checklist:

- ☐ Dispose of all hazardous waste inside plastic bag
- ☐ Clean utensils
- ☐ Turn off scale, hot plates, and lights

Notes:

PART 2: Placing samples into vacuum oven

Date: _____

Checklist:

- ☐ Pull vacuum level to 21 in Hg
- ☐ Set temperature dial to 1.5

Time placed into oven: _____

Notes:

PART 3: Taking samples out of vacuum oven

Date: _____

Oven temperature before removing: _____

Oven vacuum before removing: _____

Time oven turned off and vented: _____

Time removed from oven and temperature of oven: _____

Time removing samples from mold: _____

Heated samples? _____

Notes:

Appendix B

MAIN CODE

```
%% Notes
% Plug in the linear stage and controller
% Attach USB for PI linear stage and USB for iNet600
% Open matlab and run this main file
% Make sure the stage can move to reference position

%% CONSTANTS

% TO DO: Input sample geometry:
width = 0.166; %[inches], sample width
thickness = .067; %[inches], sample thickness
eps = 125; %[%], desired maximum strain
epsdot = 10^-3; %[1/sec] 10^-1 is the fastest the
    machine can handle
dir = ['4-05-24, 10^-3, RT, 125%'];


% Do not change
global pos_data;
global temp_data;
global load_data;
global time_data;
global datetime_starttest;
startCoarsePos = 249;
%startCoarsePos = 267.723; %use this is the position
    for monodomain samples
jog_step = 1; %[mm]
jog_velocity = 4; %[mm/sec]


% Plotting constants
```

```
30      linewidth=1.5;
31      fontsize=16;
32      fontsizemult=1.2;
33
34  if ~exist(dir,'dir')
35      mkdir(dir);
36  end
37
38  %% Connect to controller and reference stage (without
        sample connected)
39  % The stage will move to reference position of 102mm (
        the middle of the stage)
40  % This is for a single axis that is connected via USB.
41  % If you are using a different controller & stage,
        please set up in
42  % MikroMove first, then edit accordingly in
        connect_and_reference_loaner().
43
44  if ~exist('PIdevice')
45      [PIdevice, axis, Controller] =
            connect_and_reference_loaner();
46  end
47
48  disp('')
49  disp ('linear stage is done moving to reference
        position. position in mm =')
50  disp(PIdevice.qPOS(axis))
51
52
53  %% Lower stage to initial position
54  % TO DO: Put sample into top clamp before running
55
56      % Move to coarse start position and attach pullrod
57      PIdevice.VEL(axis, jog_velocity);
58      PIdevice.MOV(axis, startCoarsePos);
59      while(abs(PIdevice.qPOS(axis) - startCoarsePos) >
```

```
        0.001)
60          continue
61      end
62
63  %% Jogging: move up/down to get specimen clamped in
        position
64
65      PIdevice.VEL(axis, jog_velocity);
66      u = 'u';
67      d = 'd';
68      while (1)
69          dire = input('Move u or d? (hit enter when
                finished jogging.) ');
70          if (dire == 'u')
71              PIdevice.MOV(axis, PIdevice.qPOS(axis)-
                    jog_step);
72          elseif (dire == 'd')
73              PIdevice.MOV(axis, PIdevice.qPOS(axis)+
                    jog_step);
74          else
75              break
76          end
77      end
78
79      clear u d
80
81  %% Determine guage length
82
83      currPos = PIdevice.qPOS(axis); %[mm]
84      gaugelength_theoretical_mm = 273.6978-currPos; %[mm
            ]
85      gaugelength_theoretical_in =
            gaugelength_theoretical_mm*0.0393701;
86      gaugelength = gaugelength_theoretical_mm;
87      gaugelength_in = gaugelength_theoretical_in;
88
```

```
89  %% Set test parameters
90
91      [extension, test_velocity, tmax, epsdot] =
           test_parameters(eps, gaugelength_theoretical_in,
            'in',epsdot);
92      fprintf('epsdot = %.3e\n', epsdot)
93      fprintf('test_velocity = %.3e\n', test_velocity) %
           test_velocity in mm/sec
94
95       % extension:     mm, this is how much total
            distance you want stage
96       % to move between startPos & stopPos this is
            positive
97       % if you want stage to physically move up
98
99      crosssecarea = width*thickness*(25.4)^2; %[mm^2]
100
101     % Sample period in seconds, must be large enough
           that step size is >= 0.05 mmm
102     sample_period = input('Input desired sample period.
            Must be >= 0.5.\n')*1.0;
103     step = test_velocity*sample_period; %[mm]
104     if step < 0.05
105         error('Step size must be greater than 0.05 mm.
               Current step size is %.3\n',step)
106     end
107
108     % Configure linear stage
109     startPos = PIdevice.qPOS(axis);
110     stopPos = startPos-extension;
111
112     if (startPos > stopPos)
113         steps = [startPos:-step:stopPos, (stopPos+step)
               :step:startPos];
114     else
115         steps = [startPos:step:stopPos, (stopPos-step)
```

```
            :-step:startPos];
116     end
117
118     max(steps)
119     min(steps)
120
121
122   %% Initialize inet + preheat
123
124     if ~exist('inet')
125         inet = stephen_init_load(false, '
              tori_RTD_louisaload_jun252020'); %.prf file
126     end
127
128     %% Begin preheat
129
130     numb = 12000;
131     preheatload=NaN*zeros(size(numb));
132     preheattemp=NaN*zeros(size(numb));
133     endnum = 0;
134
135     for i = 1:numb
136         pause(2) % records temperature data every 2
              seconds
137         [preheattemp(i), preheatload(i)] =
              stephen_get_load(inet);
138         if mod(i,5) == 0 % prints temperature every 10
              seconds
139             [i/30, preheattemp(i)]
140         end
141         endnum = i;
142     end
143
144 %% Plot preheat temperature and save
145
146     preheattime = linspace(1,endnum*2,endnum);
```

```
147         figure;
148         subplot(2,1,1)
149         plot(preheattime,preheattemp)
150         xlabel('time (s)')
151         ylabel('temp (deg F)')
152         subplot(2,1,2)
153         plot(preheattime,preheatload)
154         xlabel('time (s)')
155         ylabel('load (lbs)')
156 
157         save(strcat(dir,'/preheat_data.mat'),'preheattime',
                'preheatload','preheattemp','sample_period')
158 %% MOVE
159     % Move routine
160 
161     % Extension data is saved in this variable pos_data
162     % Even if you interrupt the script using ctrl+C, it
            will save the data in
163     % this variable, also saved in a .mat file
164 
165     % Create vector of zeros to fill to speed up data
            collection
166     pos_data = NaN*zeros(size(steps));
167     temp_data = NaN*zeros(size(steps));
168     load_data = NaN*zeros(size(steps));
169     time_data = NaN*zeros(size(steps));
170 
171     PIdevice.VEL(axis, test_velocity);
172 
173     stephen_move(startPos, stopPos, step, steps,
            PIdevice, axis, inet, dir);
174 
175 %%  Calculate the actual test_velocity
176 
177     actual_test_velocity = diff(pos_data)./diff(
            time_data);
```

```
178     output_data(1,1) = test_velocity;
179     output_data(1,2) = mean(actual_test_velocity(
            actual_test_velocity>0));
180     output_data(1,3) = std(actual_test_velocity(
            actual_test_velocity>0));
181
182     output_data(1,:)
183
184 %% Plot and save raw data
185
186 N = length(pos_data);
187
188 new_pos_data = zeros(N,1);
189
190 for i=1:N
191     new_pos_data(i) = pos_data(1)-pos_data(i);
192 end
193 halfway=floor(N/2);
194
195 figure;
196 subplot(2,1,1)
197 hold on;
198 plot0a=plot(new_pos_data,load_data,'.-')
199 xlabel('extension, mm');
200 ylabel('load, lbs');
201 subplot(2,1,2)
202 plot0b=plot(pos_data, temp_data, '.-')
203 xlabel('extension, mm');
204 ylabel('temperature, degrees F');
205 saveas(plot0a,strcat(dir,'/load_extension'),'png'); %
      saves image
206 saveas(plot0b,strcat(dir,'/temp_extension'),'png'); %
      saves image
207
208 save(strcat(dir,'/extension_data.mat'),'time_data','
      pos_data','temp_data','load_data','
```

```
    datetime_starttest')

%% Plot and save stress-strain
% This is for load_data being in lbs

stress_data = load_data*.4536*9.81/(crosssecarea
    /1000^2); %convert load to stress
stress_data_zeroed = stress_data(:)-stress_data(1);
strain_data = new_pos_data/gaugelength;

figure;
plot1=plot(strain_data*100, stress_data_zeroed/1000,'.-
    ');
ax=gca;
xlabel('Strain [%]')
ylabel('Stress [kPa]')
yt=ax.YAxis;
yt.FontSize=fontsize;
xt=ax.XAxis;
xt.FontSize=fontsize;
set(gca,'linewidth',linewidth);
set(plot1,'LineWidth',linewidth);

saveas(plot1,strcat(dir,'/stress_strain'),'emf'); %
    saves image
saveas(plot1,strcat(dir,'/stress_strain'),'png'); %
    saves image

save(strcat(dir,'/stress_data.mat'),'strain_data','
    stress_data_zeroed','width','thickness','
    gaugelength_in','gaugelength','crosssecarea')
```